OXFORD

Human Molecular Genetics, 2018, Vol. 27, No. 13 2262–2275

doi: 10.1093/hmg/ddy131
Advance Access Publication Date: 10 April 2018
Original Article

ORIGINAL ARTICLE

FGF signaling deregulation is associated with early developmental skeletal defects in animal models for mucopolysaccharidosis type II (MPSII)

Stefania Bellesso[1], Marika Salvalaio[2,3], Susanna Lualdi[4], Elisa Tognon[1], Roberto Costa[5], Paola Braghetta[1], Chiara Giraudo[6], Roberto Stramare[6], Laura Rigon[2,3], Mirella Filocamo[4], Rosella Tomanin[2,3] and Enrico Moro[1,*]

[1]Department of Molecular Medicine, University of Padova, I-35121 Padova, Italy, [2]Pediatric Research Institute "Città della Speranza", I-35127 Padova, Italy, [3]Department of Women's and Children's Health, University of Padova, I-35128 Padova, Italy, [4]Centro di Diagnostica Genetica e Biochimica delle Malattie Metaboliche Giannina Gaslini Institute, Genova 16147, Italy, [5]Department of Biology, University of Padova, I-35121 Padova, Italy and [6]Department of Medicine, Radiology Unit, University of Padova, I-35128 Padova, Italy

*To whom correspondence should be addressed at: Department of Molecular Medicine, University of Padova, Via Ugo Bassi 58/B, 35121 Padova, Italy. Tel: +39 (0)498276341; Fax: +39 (0)49 8276079; Email: moroe@bio.unipd.it

Abstract

Skeletal abnormalities represent a major clinical burden in patients affected by the lysosomal storage disorder mucopolysaccharidosis type II (MPSII, OMIM #309900). While extensive research has emphasized the detrimental role of stored glycosaminoglycans (GAGs) in the bone marrow (BM), a limited understanding of primary cellular mechanisms underlying bone defects in MPSII has hampered the development of bone-targeted therapeutic strategies beyond enzyme replacement therapy (ERT). We here investigated the involvement of key signaling pathways related to the loss of iduronate-2-sulfatase activity in two different MPSII animal models, *D. rerio* and *M. musculus*. We found that FGF pathway activity is impaired during early stages of bone development in IDS knockout mice and in a newly generated Ids mutant fish. In both models the FGF signaling deregulation anticipated a slow but progressive defect in bone differentiation, regardless of any extensive GAGs storage. We also show that MPSII patient fibroblasts harboring different mutations spanning the *IDS* gene exhibit perturbed FGF signaling-related markers expression. Our work opens a new venue to discover possible druggable novel key targets in MPSII.

Introduction

Mucopolysaccharidoses are a heterogenous group of rare genetic diseases characterized by pathological accumulation of glycosaminoglycans (GAGs) into lysosomes. Although the pathogenesis has been traditionally attributed to progressive GAGs storage, recent experimental evidences support the concept that more complex mechanisms may occur. Indeed, lysosomal activity has been clearly shown to modulate a broad spectrum of cellular processes, significantly contributing to cell regulation and homeostasis (1). Furthermore, mutations altering lysosomal activity have been found to affect multiple cellular aspects, including cell death, autophagy and oxidative stress (2). The hypothesis that molecular alterations can occur before massive GAGs accumulation has been recently supported by the

Received: March 7, 2018. **Revised:** March 23, 2018. **Accepted:** March 27, 2018

discovery of very early extracellular matrix (ECM) alterations arising before the onset of gross GAGs storage (3).

Among all MPSs, mucopolysaccharidosis type II (MPSII), also called Hunter syndrome, is caused by deficiency of the lysosomal enzyme iduronate 2-sulfatase (IDS, EC 3.1.6.13), which is involved in the first step of heparan and dermatan sulfate degradative pathway. The disease has a chronic progressive course and affects multiple organs, leading to a wide range of symptoms, including hepatosplenomegaly, heart dysfunction and bone defects (4).

Over 500 different mutations spanning the *IDS* gene have been described so far, but a correlation between phenotype and genotype is still lacking (5).

We previously documented a key role of the zebrafish Ids orthologue during embryonic development, suggesting a potential involvement of the Ids enzyme in morphogens patterning and bioavailability (6).

According to the latter perspective, deposition of partially degraded GAGs in the ECM may perturb growth factors sequestering and cell signal transduction (7,8). Several examples of the detrimental role of aberrant GAGs catabolism on cell signaling activities have been reported so far (9,10), including the identification of dysregulated FGF signaling in MPS I chondrocytes and bones (11).

FGF signaling is involved in both intramembranous and endochondral ossification. Because of its crucial role during bone formation, mutations altering the FGF pathway may cause different bone diseases, such as chondrodysplasia and craniosynostosis (12). While FGF pathway has been shown to control bone growth in chondrocytes through the autophagic process (13), it appears that its transduction is finely regulated by the endolysosomal system and ECM composition (14). GAGs by binding to FGF ligands, modulate their extracellular diffusion and favor their interaction with cognate receptors (14). Indeed, heparan sulfate (HS) is necessary for FGF ligand binding to the receptor, and the peculiar GAGs sequence has been postulated to enable tissue-specific FGFs/receptors interaction (15). In particular, it has been demonstrated that the HS-sulfated residues have an essential role in ligand recognition and binding (15).

On the basis of the close functional relation between GAGs and FGF signaling, we undertook a systematic analysis of FGF signaling activity on *Ids* knockout mice and a newly generated CRISPR/CAS9-based *ids* mutant fish. Using several complementary approaches, we here document a previously unrecognized detrimental effect of defective GAGs catabolism on FGF pathway activity during bone development in Hunter syndrome animal models. We show that the loss of IDS function perturbs FGF signaling activity before the onset of skeletal alterations, without any evident GAGs accumulation. We finally show that fibroblasts from Hunter patients harboring different mutations exhibit significant misexpression of FGF pathway-related markers, thus suggesting that Hunter syndrome skeletal pathogenesis may also be ascribed to defects of developmental signaling pathways.

Results

Temporally restricted loss of zebrafish iduronate-2-sulfatase (Ids) function perturbs FGF signaling activity and FGF markers expression

We previously showed that Iduronate-2-sulfatase loss of function in zebrafish induces early developmental defects, including a misshapen facial cartilage formation and altered migration and differentiation of neural crest cells (6). To assess whether also the bone lineage was potentially affected by Ids functional impairment, we first examined Ids protein localization in the bone tissue using the transgenic reporter line *Tg(Ola.Sp7: NLS-GFP)*^{zf132}, in which the expression of the GFP reporter gene is driven by the *osterix* promoter (16). Double immunohistochemistry revealed that iduronate-2-sulfatase is localized in osteogenic regions, especially in neural crest-derived structures, i.e. opercle, cleithrum and brachiostegal ray (Supplementary Material, Fig. S1). We next screened for potential key pathways affected by Ids loss of function, by injecting a previously tested morpholino (6) in different transgenic reporter lines for different signaling pathways (FGF, Wnt, Shh, TGFβ, Notch, BMP) (17).

Using the transgenic reporter line *Tg(Dusp6: d2EGFP)*^{pt6} (18), we detected an upregulated FGF signaling in 2dpf *ids* morphant fish with respect to controls by whole-mount fluorescence microscopy, *in situ* hybridization and RT-qPCR for the reporter *d2EGFP*. To further corroborate our findings, we explored the expression of genes strictly associated with FGF signaling, including the FGF receptor *fgfr3*, FGF ligands (*fgf3* and *fgf8*) and other selected targets (*erk1*, *pea3*, *ntl*, *spry4* and *erm1*). As shown in Figure 1F–Q, we found consistent increased expression levels of all examined markers, thus confirming our preliminary findings. Notably, the FGF signaling was also consistently up-regulated in *ids* morphants at 6 dpf (data not shown), suggesting a temporarily prolonged effect of morpholino-mediated Ids loss of function on FGF pathway activity. To verify whether any FGF signaling impairment could be associated with bone developmental defects in *ids* morphants, we first performed *in vivo* Alizarin red staining on *Tg(Dusp6: d2EGFP)*^{pt6} and analyzed cephalic bones at 6 dpf by confocal microscopy. As shown in Supplementary Material, Figure S2, we noticed that the opercle of *Tg(Dusp6: d2EGFP)*^{pt6} fish was positive for Alizarin red staining. We next assessed target bone markers (*runx2b* and *col10a1*) expression by *in situ* hybridization in *ids* morphants and compared it with that of age-matched control larvae at 2 and 3 dpf. We preliminarily found that fish morphants exhibit upregulation of *runx2b* and downregulation of *col10a1* in the opercle, cleithrum and brachiostegal ray, when compared with age matched controls (data not shown). We, therefore, could conclude that transient *ids* knock-down perturbs FGF signaling activity and affect the expression of target bone markers.

Generation of CRISPR/Cas9-induced *ids* mutant fish

To better elucidate the association of deregulated FGF pathway with Ids loss of function-related bone defects at late life stages, we generated a stable *ids* mutant using the CRISPR/Cas9 technology. We successfully targeted a sequence of *ids* exon2, creating a 5 base pair deletion (deleted sequence TCACT, from nucleotide 241 to nucleotide 245) very close to the active residue Cysteine 78 (Fig. 2). As verified by sequencing the DNA from different independent larvae obtained by mutant carriers and from the offspring of inbred carriers after several generations, we were able to identify a stable *ids* mutant line, henceforth referred to as ids^{ia200}. In mutant fish, the 5 bp deletion causes a frameshift altering the protein sequence from amino acid 82 (Fig. 2A) and leading to the generation of a premature stop codon at the amino acid in position 118.

Since the truncated protein was supposed to be non-functional, we verified Ids enzymatic activity in mutant larvae. As shown in Figure 2B, protein crude extracts from homozygous mutants, obtained from inbred ids$^{ia200/ia200}$ fish exhibited

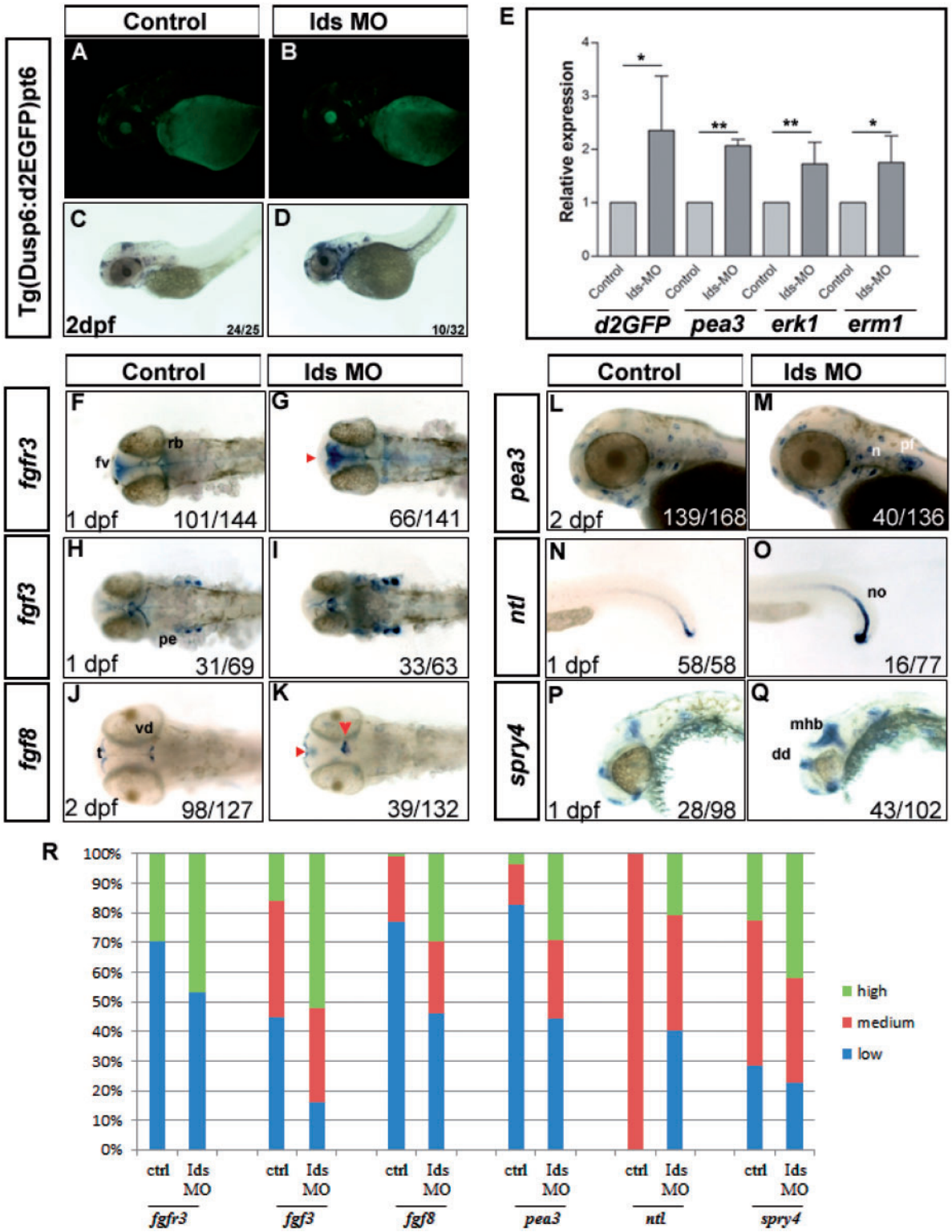

Figure 1. FGF signaling is impaired in Ids morphant fish. (**A, B**) Representative 2dpf *Tg(Dusp6: d2EGFP)*^{pt6} morphant fish (A) showing increased FGF reporter activity when compared with a mismatch control (B). (**C, D**) Representative *in situ* hybridization on *Tg(Dusp6: d2EGFP)*^{pt6} morphant and control larvae with a d2GFP-specific antisense riboprobe, demonstrating increased d2GFP transcripts in Ids morphants. (**E**) RT-qPCR analysis for d2GFP and FGF targets (*pea3*, *erk1* and *erm1*) mRNAs confirmed the upregulation of FGF pathway activity occurring in Ids morphants when compared with age-matched controls. Data are expressed as mean ± SD of four independent experiments ($n = 50$ larvae for each condition) (*$P < 0.05$, **$P < 0.02$; *t*-test). (**F–Q**) Ids morphants display increased FGF receptor fgfr3, ligands (*fgf3* and *fgf8*) and targets (*pea3*, *ntl* and *spry4*) expression with respect to controls. All *in situ* hybridization images are representative of three independent experiments. Values in each panel represent the fraction of larvae with the reported gene expression intensity. A-D and L-Q are lateral views with anterior to the left. F-K are dorsal views with anterior to the left. dd, dorsal diencephalon; fv, forebrain ventricular zone; mhb, midbrain hindbrain boundary; n, neuromast; no, notochord; pe, pharyngeal endoderm; pf, pectoral fin; rb, rhombomere boundaries; t, telencephalon; vd, ventral diencephalon. (**R**). Bar graph showing the range of detected *in situ* hybridization intensities for the target genes in control and morphant larvae. The terms 'high,' 'medium' and 'low' have been arbitrarily designated to identify the different classes of gene expression intensity.

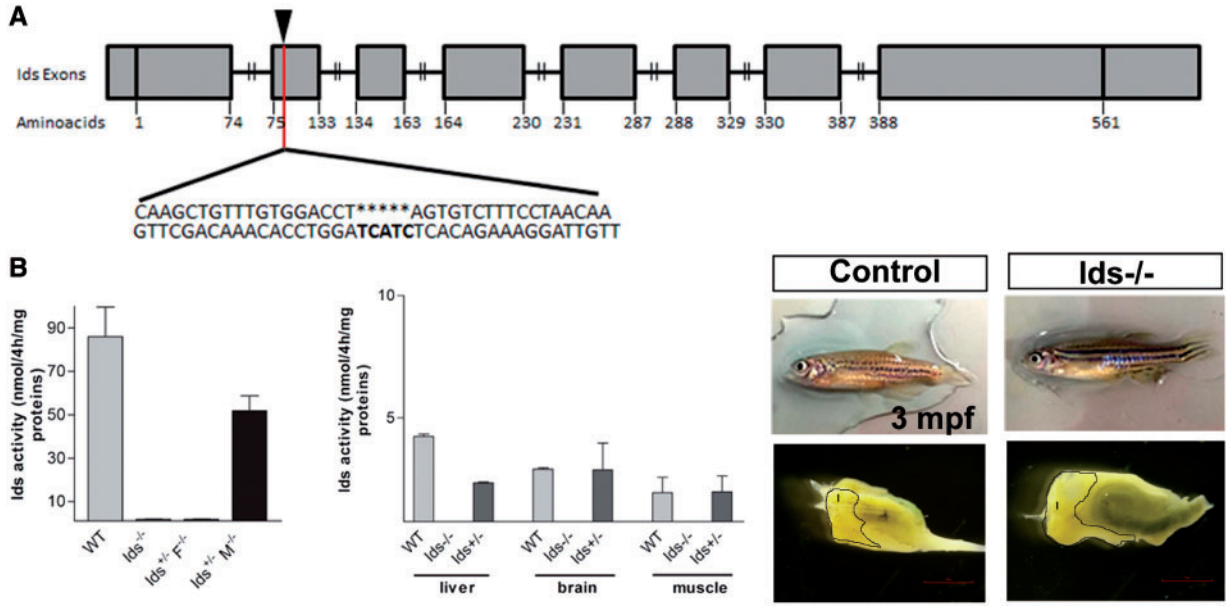

Figure 2. Generation and characterization of the zebrafish stable Ids mutant line, ids^{ia200}. For graphical reasons homozygous fish and heterozygous carriers have been designated Ids$^{-/-}$ and Ids$^{+/-}$, respectively. (**A**) Genomic structure of the zebrafish *ids* gene. Exons are depicted by grey boxes, with the progressively numbered aminoacids. The 5 bp deletion (sequence CTACT) in Ids exon2 generated by CRISPR/Cas9 is indicated below. (**B**, **C**) Iduronate-2-sulfatase activity assays performed in whole lysates (B) and isolated organs (liver, brain, muscle) (C) from 2 dpf and 3-month-old wild-type, homozygous ids$^{ia200/ia200}$ and heterozygous ids$^{ia200/+}$ fish, respectively. Data are derived from three independent measurements ($n = 100$ larvae for each condition). (**D**) Representative 3-month-old control and ids$^{ia200/ia200}$ fish and their isolated liver. The enlarged liver (l) size in the homozygous mutant is depicted by the dotted line ($n = 5$ fish for each condition).

negligible enzymatic activity when compared with control WT protein extracts. Heterozygous ids$^{ia200/+}$ fish, generated from a cross between homozygous female mutants and WT males, showed the same Ids enzyme activity of ids$^{ia200/ia200}$ fish, while heterozygous fish ids$^{ia200/+}$, obtained from a cross between WT females and ids$^{ia200/ia200}$ males, displayed a 60% reduction of enzymatic activity when compared with that of age-matched WT. Notably, enzymatic activity in heterozygous larvae derived from homozygous mutant females and WT males were still significantly decreased at 9 dpf, when compared with age-matched wild-type fish (data not shown). Enzyme activity assays were also performed in isolated tissues (brain, liver and muscle) from 3-month-old ids$^{ia200/ia200}$, ids$^{ia200/+}$ and WT fish. When compared with extracts from whole larvae, the range of measured enzymatic activity values from isolated tissues was much more reduced. However, in all examined organs from ids$^{ia200/ia200}$ fish there was no detectable enzyme activity. On the contrary, ids$^{ia200/+}$ fish exhibited the same enzymatic activity of WT fish in brain and muscle, and half enzymatic activity in liver when compared with age-matched control tissues (Fig. 2C).

Since one of the most evident pathological manifestations in Hunter patients is hepatomegaly, we examined whether ids$^{ia200/ia200}$ fish recapitulate the same phenotype. For this purpose, the liver from 3-month-old ids$^{ia200/ia200}$ and WT fish were isolated and evaluated under stereomicroscope. As shown in Figure 2D, liver size in mutant fish was increased when compared with age-matched wild-type fish.

We, therefore, could conclude that the ids$^{ia200/200}$ line represents a full loss of function mutant, displaying a characteristic feature (hepatomegaly) of Hunter syndrome. Moreover, given the prolonged significant reduction of enzymatic activity in ids$^{ia200/+}$ larvae, derived from homozygous mutant females and wild-type males, we could infer that the maternal enzyme contribution is substantial in the first developmental stages, as well as at later life stages.

FGF signaling perturbation occurs in *ids* mutant fish during early development and is recapitulated in the bone compartment during adult stages

Considering the previously detected FGF signaling dysregulation in *ids* morphants, we sought to verify whether the same cell signaling defects were present in stable *ids* mutant fish. Towards this aim, we crossed the ids$^{ia200/ia200}$ fish with the *Tg(Dusp6: d2EGFP)*^{pt6} and analyzed the offspring obtained from inbred transgenic mutant carriers. As shown in Figure 3A and B, we detected regions of significantly decreased transgene reporter expression by both confocal microscopy analysis and RT-qPCR of the d2GFP reporter marker. To further confirm the FGF signaling deregulation in ids$^{ia200/ia200}$fish, we carried out RT-qPCRs for FGF signaling targets (*pea3*, *erk1*, *erm*) in pooled RNA extracts from 2 dpf ids$^{ia200/ia200}$ fish. In several independent experiments we consistently found a significant decrease of all examined FGF targets in Ids mutants, when compared with age-matched control fish. To assess whether the FGF signaling impairment was persistent at late life stages, we isolated bone tissue (from skull, opercle and caudal fin) from 3-month-old ids$^{ia200/ia200}$ and control WT siblings and analyzed FGF targets (*pea3*, *erk1*, *dusp6*) by means of RT-qPCR.

As shown in Figure 3C–E, we found reduced expression of FGF markers in all examined bone tissues from Ids mutants, when compared with age-matched controls.

These results suggest that a FGF signaling dysregulation is triggered by Ids loss of function in fish during early developmental stages and persistently maintained at the bone level in adult mutant fish.

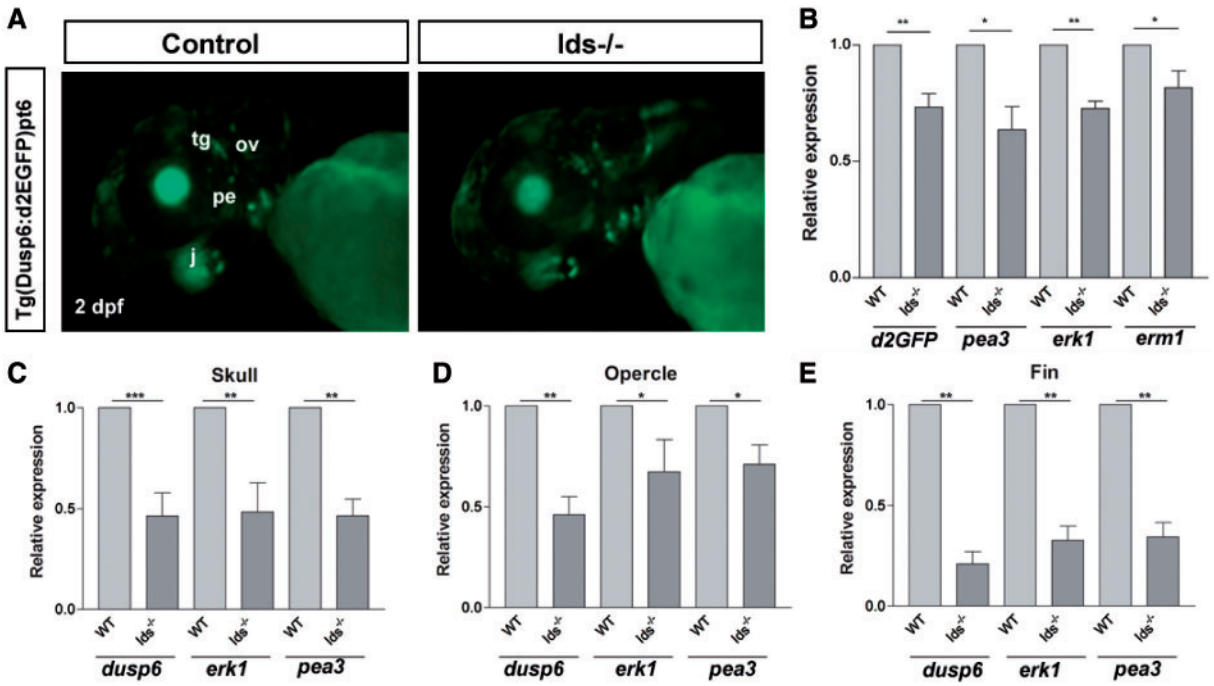

Figure 3. FGF signaling is dysregulated in ids$^{ia200/ia200}$ mutant fish. (**A**) Representative *Tg(Dusp6: d2EGFP)*^{pt6} WT and ids$^{ia200/ia200}$ fish at 2 dpf. Mutant fish exhibit regions of decreased GFP expression when compared with age-matched controls. j, jaw; ot, otic vesicle; pe, pharyngeal endoderm; tg, trigeminal ganglia. (**B**) Bar graph showing significantly reduced expression levels for the indicated markers measured by RT-qPCR in 2 dpf *Tg(Dusp6: d2EGFP)*^{pt6} ids$^{ia200/ia200}$ fish when compared with those of control fish. ($n = 50$ larvae for each condition). Data represent the mean ± SD of four independent experiments (*$P < 0.05$, **$P < 0.02$; *t*-test). (**C–E**) Bar graphs depicting the RT-qPCRs-based quantitative decrease of indicated FGF markers in isolated bone samples from 12-month-old mutant and control fish ($n = 5$ fish for each condition). Data are expressed as mean ± SD of four independent experiments (*$P < 0.05$, **$P < 0.02$; *t*-test).

Impaired expression of skeletal-related markers occur in stable ids mutant fish at both early and late life stages

We previously showed that transient Ids functional knockdown affects the neural crest-cell lineage and disrupts the craniofacial cartilages development during larval stages (6).

To evaluate whether Ids loss of function could negatively affect bone development at late life stages, we crossed the ids$^{ia200/ia200}$ fish with *Tg(Col2a1aBAC: mCherry)*^{hu5900} (19) and *Tg(Ola.Sp7: NLS-GFP)*^{zf132} (16) and analyzed by confocal microscopy the offspring from incrossed transgenic mutant carriers. As regards the *Tg(Col2a1aBAC: mCherry)*^{hu5900} line, from 4dpf to 15dpf a transgene reporter activity increase was evident in WT fish, while at 7dpf in ids$^{ia200/ia200}$ fish we measured a statistically significant rapid increase of transgene expression, followed by its rapid decline (Supplementary Material, Fig. S3A). Similar results were obtained when analyzing the ids$^{ia200/ia200}$ fish in the *Tg(Ola.Sp7: NLS-GFP)*^{zf132} background. While from 4 to 15 dpf WT fish displayed increased transgene expression in the opercle and brachiostegal regions, we detected a significant decrease of transgene expression in age-matched mutants (Supplementary Material, Fig. S3B and data not shown). By Alizarin red staining we next evaluated the degree of bone mineralization affected by Ids loss of function. In both 6 and 15 dpf ids$^{ia200/ia200}$ fish we did not find substantial difference between homozygous mutants and age-matched control fish (Fig. 4A).

To extend our preliminary observations to adult stages, we isolated different bone structures (skull, opercle and caudal fin) from 12-month-old ids$^{ia200/ia200}$ and age-matched control siblings and analyzed the expression of *col2a1*, *col10a1*, *osx* (*sp7*) and *bglap* markers by RT-qPCR. As shown in Figure 4B, we detected significantly reduced *osx* mRNAs in all examined tissues of ids$^{ia200/ia200}$, while, according to the analyzed skeletal element, we could measure a variable degree of differential expression of the other markers between the two genotypes. Western blot analysis performed on protein lysates obtained from the skull and opercle of ids$^{ia200/ia200}$ fish partially confirmed the results by RT-qPCR for *bglap*. To further investigate the impact of Ids functional impairment on the skeletal maintenance, we carried out Micro-computed tomography (MicroCT) analysis on aged ids$^{ia200/ia200}$ and controls. As shown in Figure 4C, MicroCT analysis revealed the recurrent presence of skeletal deformities in 15-month-old controls. In particular, ids$^{ia200/ia200}$ fish displayed anomalies in the curvature of the spine such as kyphosis (Fig. 4B, upper right panel) and scoliosis, including also a rotational component (Fig. 4B, lower right panel). A detailed examination of the anomalous curvature obtained with a curvilinear multiplanar reconstruction (MPR) and axial images of three single vertebrae (Fig. 4C) in the area affected by scoliosis of the mutant fish demonstrated additionally to the sideways curve, a higher vertebral density, presumably due to a compressive phenomenon.

These results, therefore, suggest that in stable Ids mutants the bone differentiation program is already negatively affected during early larval stages, preceding the onset of profound skeletal abnormalities which are evident at late life stages.

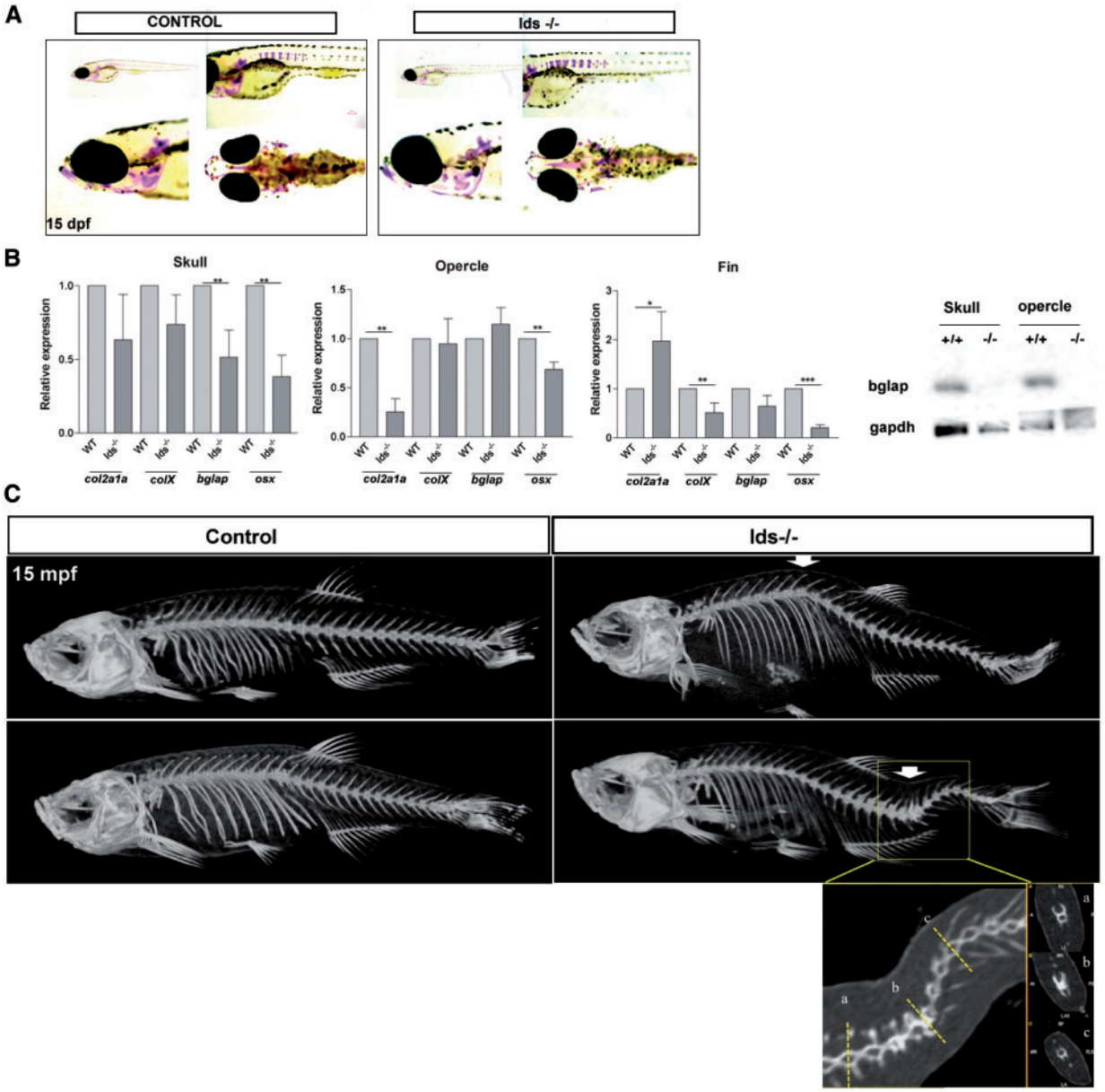

Figure 4. Ids loss of function induces progressive bone developmental alterations in zebrafish. (**A**) Representative Alizarin red stained 15 dpf control and ids$^{ia200/ia200}$ fish. Homozygous mutants do not display overt alterations of bone mineralization when compared with age-matched controls. All images are lateral views with anterior to the left, except the one at the bottom right in each panel, which is a ventral view with anterior to the left ($n = 10$ larvae for each condition). (**B**) Bar graphs showing the RT-qPCRs-based quantitative analysis of indicated bone-specific markers in isolated skeletal samples from 12-month-old mutant and control fish. A significant downregulation of *osterix* (*Osx*) expression is detected in all examined tissues from fish mutants when compared with age-matched controls ($n = 5$ for each condition). Data are expressed as mean ± SD of four independent experiments (*$P < 0.05$, **$P < 0.02$, ***$P < 0.002$; *t*-test). A representative western blot analysis ($N = 3$) for bglap in fish skull and opercle bone extracts is depicted. (**C**) Representative 3D reconstructions of 15-month-old (15 mpf) WT and *ids* mutant fish. Mutant fish display kyphosis of the spine (white arrow above) and scoliosis (white arrow below), while WT samples do not show any anomaly. The yellow square represent a high magnification of three single vertebrae (a, b and c) in the area affected by scoliosis and it is obtained with a curvilinear MPR and axial images. In the point of rotation (b) the vertebral body demonstrates a higher density ($n = 4$ fish for each condition).

IDS knockout mice exhibit defective FGF signaling and reduced bone-related markers expression in appendicular bone at postnatal stages

To further support the key role of FGF signaling dysregulation in the onset of bone defects in MPSII, we extended our investigation to IDS knockout mice (20). This mouse model carries a deletion of exon 4 and part of exon 5 of the *Ids* gene, leading to the transduction of a non-functional enzyme. According to the previously performed phenotypic characterization (20), IDS-KO mice at birth and during early stages of development didn't display any macroscopic morphological alteration, when compared with age-matched WT mice (Fig. 5A). We, however, chose to analyze 1 week and 2 weeks old IDS-KO mice, which did not exhibit evident GAGs accumulation and macroscopic bone defects (Supplementary Material, Fig. S4A). Moreover, at both stages we did not find significant body weight differences between KO mice and age-matched controls (Supplementary Material, Fig. S4B). However, a thorough analysis showed early

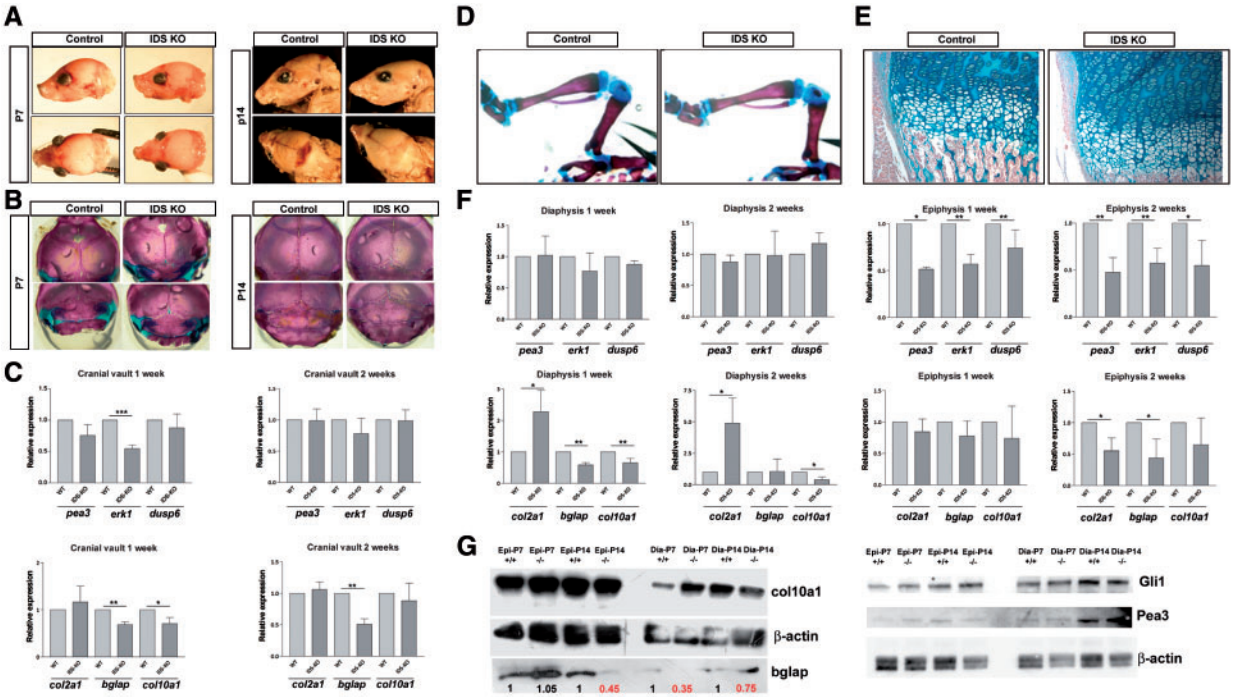

Figure 5. IDS KO mice show early FGF signaling and skeletal markers dysregulation. (**A**) Representative skull of P7 (left panel) and P14 (right panel) IDS knockout and control mice. P7 KO mice display a flattened skull when compared with that of age-matched controls. (**B**) Representative Alcian blue-Alizarin red stained cranial vault of P7 (left) and P14 (right) WT and IDS-KO mice. Knockout mice exhibit jagged skull sutures when compared with age-matched controls. (**C**) Bar graphs depicting the RT-qPCR analysis for FGF-related markers (top panels) and bone markers (bottom) performed in cranial vault samples from 1 week (left panels) and 2 weeks old (right panels) IDS-KO and WT mice. Data are expressed as mean ± SD of four independent experiments (**$P < 0.02$, ***$P < 0.002$; *t*-test). (**D**, **E**) Representative Alcian blue-Alizarin red stained long bones. In E a representative tibial bone section of P7 WT and IDS-KO mice is depicted. Knockout mice do not show any early gross long bone deformities when compared with age-matched controls. (**F**) Bar graphs showing the RT-qPCR analysis for FGF signaling targets (*Pea3*, *Erk1* and *Dusp6*) (top) and bone-related markers (*Col2a1*, *Bglap* and *Col10a1*) performed in the femur diaphysis and epiphysis of 1 week and 2 weeks old IDS-KO and WT mice ($n = 4$ mice for each condition). Data are expressed as mean ± SD of four independent experiments (*$P < 0.05$, **$P < 0.02$; t-test). (**G**) Representative western blot analysis showing the protein levels for the analyzed markers in bone tibial extracts (epiphysis and diaphysis) from control and IDS KO mice ($N = 4$ for each condition). Numbers in red depict the quantitative decrease for Bglap levels detected in epiphysis (P14) and diaphysis (P7 and P14) of KO mice when compared with age-matched controls.

alterations in the cranial vault size and shape of KO mice when compared with that of age-matched controls. In particular, 1-week-old KO mice displayed a flattened skull, while at 2 weeks the skull height was significantly increased when compared with that of age-matched controls (Supplementary Material, Fig. S4C). Moreover, IDS-KO mice exhibited jagged skull sutures when compared with age-matched WT siblings (Fig. 5B).

No significant differences were indeed detected in long bones length and size of 1 week and 2 weeks old IDS-KO mice, when compared with age-matched controls (Supplementary Material, Fig. S5A–F and data not shown). To better detect subtle defects in bone morphogenesis at early stages, we performed Alcian blue/Alizarin red staining of serial tibial and femoral bone sections, but we did not find evident differences between KO mice and age-matched control samples (Fig. 5D and E). We next evaluated FGF signaling-related markers (*Pea3, Dusp6, Erk1*) by RT-qPCR on total RNA extracts from the cranial vault, diaphysis and epiphysis of 1 week and 2 weeks old KO and control mice. We found that all three markers were significantly reduced in the epiphysis of KO mice (Fig. 5F). We, therefore, tested the expression levels of bone-related markers in the same samples and we detected a significant decrease of *Bglap* expression in the cranial vault and diaphysis of 1-week-old KO mice with respect to controls. A significantly reduced *Bglap* expression was also measured in the cranial vault and epiphysis of 2 weeks-old KO mice when compared with age-matched controls.

Matching results were obtained by western blot analysis for Bglap in protein extracts from control and KO mice tibia samples (Fig. 5G), as well by immunohistochemistry using antibodies toward Pea3 and Col2 on paraffin sections from the epiphyseal plate of KO mice tibia when compared with those of age-matched controls (Supplementary Material, Fig. S6A and B). In particular, for Col2 although the overall amount of immunopositive cells was not significantly different between control and IDS-KO mice in agreement with RT-qPCR data, we found that in KO mice Col2 was mainly expressed in the proliferating zone, while in control mice it was equally distributed among the all three zones (proliferating, pre-hypertrophic and hypertrophic).

To verify whether the decrease of *Bglap* expression in the KO mice bone samples could be related to an inflammatory process, we examined the expression profile of two key pro-inflammatory cytokines, IL1β and TNFα, which have been shown to increase during the onset of MPS-related osteoarticular defects (21). We did not find, however, any evidence of increased expression in all examined samples of both 1-week and 2-week-old KO mice when compared with those of age-matched controls (Supplementary Material, Fig. S7).

We could, therefore, conclude that at least in the epiphyseal region of the bones, the loss of *Ids* function is associated with a significant reduction of target FGF markers and *Bglap* expression at very early postnatal stages. Moreover, the

Table 1. List of Hunter patients recruited in the study and their detected mutations in the *IDS* gene

Patient	Mutation (protein)[a]	Type of mutation	Localization
A1	p.Pro4Serfs*43	Non-sense mutation	N-terminal
A2	p.Arg8*		
A3	p.Trp12*		
A4	p.Gln66*		
A5	p.Gln80*		
A6	p.Tyr103*		
B1	p.Ser117del	Deletion	
C1	p.Asn63Asp	Missense mutation	
C2	p.Arg88His		
C3	p.Arg88Pro		
C4	p.Pro120Arg		
D1	p.Leu279*	Non-sense mutation	C-terminal
D2	p.Leu359*		
D3	p.Arg443*		
E1	p.Cys422Arg	Missense mutation	
E2	p.Cys422Arg		
E3	p.Pro467Leu		
E4	p.Arg468Gln		
E5	p.Arg468Gln		
E6	p.Arg468Gln		
E7	p.Arg468Gln		

decreased osteogenic *Bglap* levels do not appear to be related to increased pro-inflammatory cytokine expression.

Misexpression of FGF signaling markers is detected in Hunter syndrome patients' fibroblasts

To verify whether any hallmark of FGF signaling dysregulation could be detected also in MPSII patients, we performed RT-qPCR for target FGF markers (*DUSP6*, and *PEA3*) on fibroblast RNAs from a selected cohort of Hunter patients and compared their quantitative expression profile with that of unaffected relatives' fibroblast RNA (Table 1). As shown in Figure 6 we found 14 out of 21 (66.7%) patients exhibited significantly reduced *DUSP6* expression levels, while for *PEA3*, 8 out of 21 (38.1%) displayed decreased mRNA levels. As regards the correlation between the localization of the mutation and the FGF marker misexpression, we found that 9 out of 11 (81.8%) patients carrying an N-terminal mutation (patient A1-C4, Table 1) exhibited significantly decreased *DUSP6* mRNA levels, when compared with controls. On the other hand, only 5 out of 11 (45.4%) patients with the same N-terminal mutations displayed decreased *PEA3* mRNA levels. For patients with C-terminal mutations (D1-E7, Table 1), significantly decreased mRNA levels for *DUSP6* and *PEA3* were detected only in 5 out of 10 (50%) patients and 3 out of 10 (30%) patients, respectively. Due to limited availability of clinical information, we were not able to precisely classify each patient according to disease severity.

Therefore, despite our limited analysis in a small cohort of patients, we could conclude that at least IDS N-terminal mutations are related to significantly decreased DUSP6 mRNA levels in a high proportion (81.8%) of affected patients.

Discussion

The concerted action of secreted growth factor and morphogens together with ECM components (proteoglycans, collagens, non-collagenous proteins and soluble enzymes) orchestrates key cellular processes including cell differentiation (22). Alterations in the ECM composition have been widely associated with pathological conditions, including lysosomal storage disorders (LSDs), characterized by a complex range of disease manifestations (8,23). Among several affected tissues, bones and skeletal-related components (cartilages and tendons) are significantly affected by perturbations of the ECM, especially during early developmental stages (24). In the past decades, lysosomal diseases, including MPSs, have been collectively attributed to the progressive storage of undegraded substrates. Recently, however, new pathogenic cascades, such as autophagic defects and ECM-related protein alterations have been postulated to underpin the onset of some pathological manifestations in LSDs (3,25). By using the combination of different techniques on two different animal models (zebrafish and mouse) for MPSII, we have here documented a novel unexplored association between FGF signaling impairment and Hunter syndrome-related skeletal manifestations.

Using both a transient and a newly generated stable Ids loss of function fish model, we have demonstrated that a subtle significant impairment of the FGF pathway and the consequent misexpression of FGF target genes during early life stages precede the onset of irreversible skeletal alterations. These results have been further confirmed in a well-characterized mouse model for MPSII (20) during postnatal stages, suggesting a potential evolutionary conserved mechanism responsible for the skeletal alterations occurring in vertebrate animal models for MPSII.

The identification of an FGF pathway dysregulation before the onset of bone defects in MPSII strongly supports the general concept that the FGF/FGF receptor (FGFR) axis controls the skeletal growth, maintenance and remodeling (26). Although we are aware that other major key signaling pathways, including TGFβ, BMP, Shh and canonical Wnt, may be responsible for the detected skeletal defects, our data suggest that impairment of the FGF pathway may potentially contribute to the primary onset of both endochondral and intramembranous ossification defects. We have in fact noticed that either *col2a1*, *col10a1* or *osterix* (Sp7) expression, as well as the relative transgenes were affected since early developmental stages in the fish models, before any overt massive GAGs accumulation. Comparably, the expression of *Col10a1* and *Bglap* was significantly reduced in the diaphysis of 1-week-old IDS-KO mice, when no Alcian-blue detectable GAGs were observed.

These results were consistent with a previously documented role of Ids during embryonic development (6), and in agreement with our very recent findings on the cardiac lineages defects observed in MPSII animal models (27), we may now be able to more generally include well-defined cell signaling defects among pathogenic mechanisms underlying MPSII, challenging the primary storage GAG-centric perspective.

A key aspect of our findings is the detection of FGF pathways and bone markers misexpression in a window of time when no evident skeletal defects are seen in both fish mutants and KO mice. This is consistent with the previously documented occurrence of early ECM–related molecular changes detected in the femoral heads of alpha-L-iduronidase (IDUA) KO mice associated with the later onset of bone and joint disease in MPSI (3). Nonetheless, this evidence agrees with the clinical benefits obtained by early ERT-based treatment, as recommended by the European guidelines (28,29).

To ascertain whether FGF signaling-related molecular changes could be a hallmark in Hunter patients, we undertook a preliminary systematic analysis of representative FGF markers (DUSP6 and PEA3) in a selected cohort of patients and healthy

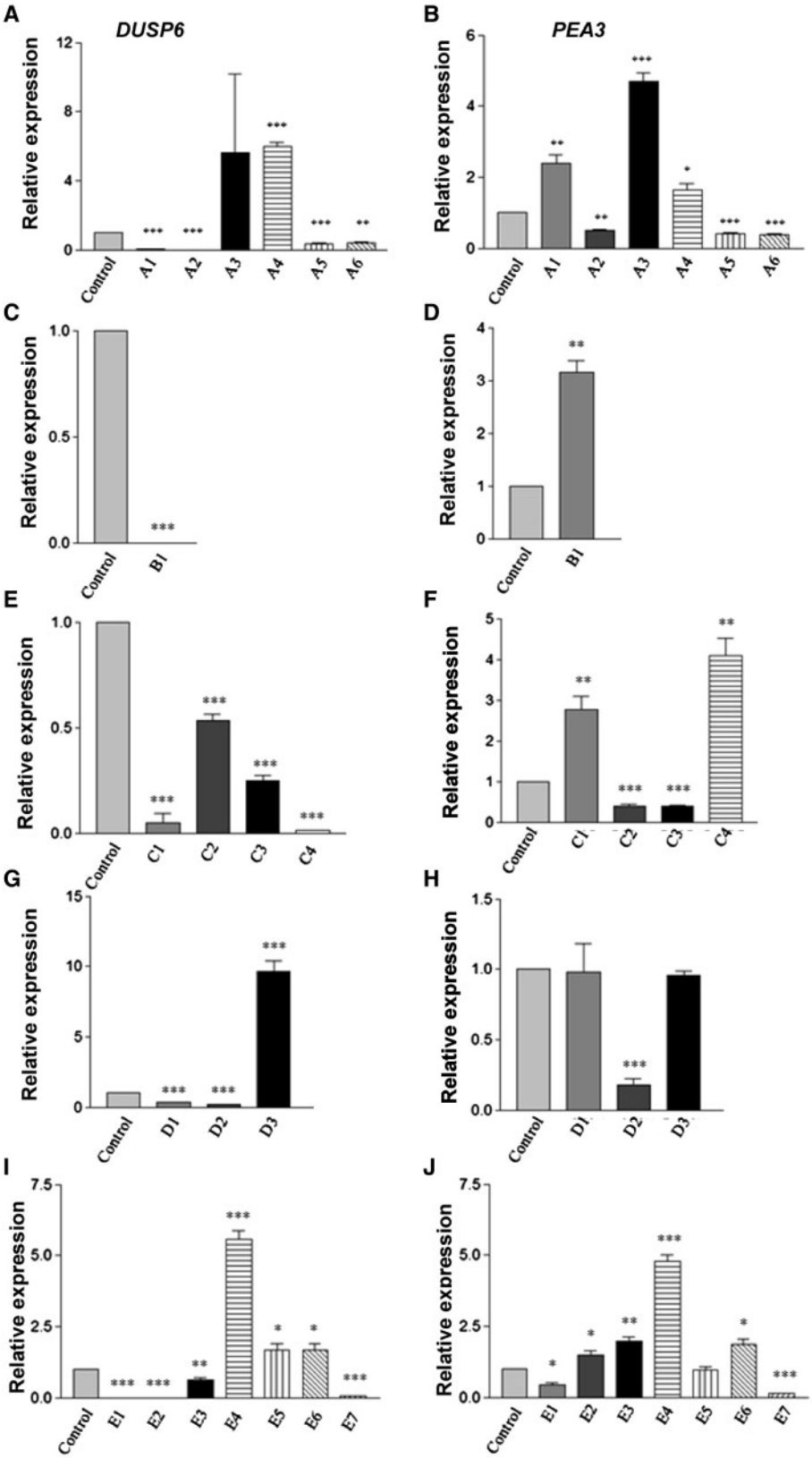

Figure 6. Reduced FGF pathway markers in Hunter patients' fibroblasts. (**A–J**) Bar graphs depicting the RT-qPCR-based quantification of FGF-related markers PEA3 and DUSP6 expression in fibroblast samples from patients harboring different iduronate-2-sulfatase mutations and healthy controls. All samples have been grouped according to the type of mutation and the localization of the IDS mutation in: N-terminal non-sense mutation (A, B), N-terminal deletion (C, D), N-terminal missense mutation (E, F), C-terminal non-sense mutation (G, H) and C-terminal missense mutation (I, J). Data are expressed as mean ± SD of four independent experiments (*$P < 0.05$, **$P < 0.02$, ***$P < 0.002$; *t*-test).

controls. The identification of reduced *DUSP6* mRNA levels in fibroblasts samples from patients with N-terminal IDS mutations may suggest a potential link between IDS loss of function and FGF signaling pathway dysregulation. Indeed, the more reduced frequency of PEA3 downregulation in Hunter patients' samples may be explained by the complex transcriptional regulation of PEA3 expression by the canonical Wnt pathway, in agreement with the previously described presence of TCF binding sites in the PEA3 promoter region (30).

We are aware that the use of fibroblasts RNA as template for RT-qPCR analysis would not be appropriate, since for both animal models we extrapolated the same results by using bone tissue RNA as template. However, the lack of bone biopsies together with evident ethical concerns prevented us to carry out any transcriptional analysis in bone tissues from Hunter patients. By the way, from our transcriptional analysis of human samples we noticed that patients harboring mutations in the same *IDS* region (e.g. N-terminus) or even patients with the same mutation (R458Q) exhibit different *DUSP6* expression profile. This is consistent with poorly understood pathogenic mechanisms, involving the iduronate-2-sulfate enzyme itself. Considering that all patients did not exhibit any residual enzymatic activity, different hypothesis could be plausibly raised to justify the different FGF signaling-related molecular profile. First, the occurrence of inter-patients genetic background differences may underlie a different cell signaling response to IDS enzymatic deprivation, as a consequence of complex GAGs rearrangements of the ECM milieu, due to heparan and dermatan sulfates storage. This hypothesis would imply in agreement with previous observations that even subtle changes in the heparan and dermatan sulfate of the ECM composition due to IDS dysfunction may be sufficient to disrupt the physiological activity of FGF ligands and their cognate receptors (31). A very recent investigation supporting this scenario has been documented in Hurler syndrome cell lines (11). A second arguable hypothesis would, indeed, consider a potential direct or indirect physical interaction between the IDS enzyme itself and one or more FGF signaling transducers. We have, in fact, noticed that while the Ids morpholino targeting the ATG translation initiation site in zebrafish produces an upregulation of the FGF pathway, a splicing site mutation targeting a more downstream region in Ids exon 2 produces a downregulation of the same pathway. Similarly IDS-KO mice which harbor a deletion of exon 4 and part of exon 5 in the *Ids* gene exhibit the same downregulation of the FGF pathway. The latter hypothesis cannot be ruled out as during signal transduction, some of the FGF ligands and receptors (FGF1/FGFR4) are sorted through the endosomal/lysosomal pathway, thereby potentially enabling the physical contact between lysosomal enzymes and cell signaling transducers (32).

In conclusion, although a more detailed analysis of FGF signaling transduction is needed to clarify the level at which IDS loss of function may interfere with FGF pathway activity, it is plausible to speculate that in the onset of skeletal defects, a potential involvement of the FGF may be evoked thereby supporting the involvement of cell signaling defects in Hunter syndrome pathogenesis.

Materials and Methods

Morpholino-based *ids* knockdown

Transient Ids knockdown was obtained using a previously described translation blocking morpholino (6). The microinjection was performed resuspeding the morpholino oligo in Danieau buffer [8 mM NaCl, 0, 7 mM KCl, 0, 4 mM $MgSO_4$, 0, 6 mM $Ca(NO_3)$, 2, 5 mM HEPES, pH 7.6] and Red Phenol (Sigma, Milan, Italy) at the working concentration. Microinjections were performed in collected one-cell stage embryos under a light microscope. Pigmentation was prevented using a 0.003% 1-phenyl-2-thiourea solution in the first 24 h.

Immunohistochemistry

For whole-mount immunohistochemistry a previously published protocol was considered (33). Zebrafish were fixed in 4% PFA and stored in a 30% sucrose solution. Primary antibody (Iduronate-2-sulfatase 1: 100, Novus Biologicals, Littleton, CO, USA) (GFP 1: 100, ThermoFisher Scientific, Monza, Italy) was incubated 3 days at 4°C, while the secondary antibody (Goat anti-Mouse IgG Fc TRITC conjugate 1: 200, ThermoFisher Scientific, Monza, Italy) [Goat anti-Rabbit IgG (H + L) FITC conjugate 1: 200, ThermoFisher Scientific, Monza, Italy] was incubated 2 days at 4°C in the dark. Immunolabeled fish were mounted onto glass slides using a Fluoro-mount medium (Thermofisher, Italy).

Zebrafish lines and mouse

Zebrafish larvae were kept for the first 5 days in Petri dishes, then maintained at 28°C for the next stages in 5 l tanks filled with fish water at neutral pH, according to standard procedures (http://ZFIN.org).

Tg(Col2a1aBAC: mCherry)^{hu5900} transgenic fish express the fluorescent protein mCherry under the control of a Collagen 2-specific promoter (19). In *Tg(Ola.Sp7: NLS-GFP)*^{zf132} the GFP reporter protein coding sequence is under the control of a Osterix-specific promoter (34). *Tg(Dusp6: d2EGFP)*^{pt6} transgenic reporter line express the destabilized d2GFP under the control of Dusp6 promoter (18).

IDS-KO mouse model for Hunter syndrome was already described previously (20).

All animal manipulation procedures were conducted according to the Local Ethical Committee at the University of Padova and National Agency (Italian Ministry of Health, project no. 77 and 78/2013).

In situ hybridization

Whole mount *in situ* hybridizations were performed in larvae fixed at different developmental stages by 4% buffered *p*-formaldehyde in PBS (PFA), using a previously described protocol (35). The following digoxygenin-labeled antisense riboprobes were used: *fgf3* (36), *ntl* (37), *pea3* (38), *fgf8* (39), *spry4* and *fgfr3* (40). A GFP antisense riboprobe was generated from a Tol2 middle entry vector containing the GFP cassette.

Enzymatic assay

Samples were obtained by homogenizing larvae or tissues in ice with a lysis buffer (ThermoFisher Scientific, Monza, Italy). Debris were pelleted twice by centrifugation at 4°C and supernatants were collected and assayed for total protein concentration (mg/ml) by the Bio-Rad Protein Assay Dye Reagent Concentrate (Biorad, Milan, Italy).

Iduronate 2-sulfatase activity was determined by a two-step fluorimetric assay using the substrate 4-Methylumbelliferyl-α-L-Idopyranosiduronic Acid 2-sulfate (MU-α-ldoA-2S, Moscerdam

Substrates, Oegstgeest, Netherlands). Results were obtained using 4-methylumbelliferone as a standard and were normalized for total protein levels. Ids activity was expressed as 1 nmol of MU-α-ldoA-2S substrate hydrolysed in 4 h per mg total proteins (nmol/4 h/mg).

RT-qPCR

For whole RNA extracts pools of 50 fish larvae were used for each independent experiment. For bone samples from adult fish and mice at post-natal stages four different animals were euthanized and skeletal tissues isolated according to standard procedures. Briefly, zebrafish larvae, bone samples and mouse bone samples were homogenized in Trizol reagent (ThermoFisher Scientific, Monza, Italy) and total RNA was isolated according to manufacturer's instructions. RNAs were resuspended in 20 μl of RNAse-free water and then quantified by Nanodrop 1000 (ThermoFisher Scientific, Monza, Italy). A total of 2 μg of RNA were reverse transcribed using a SuperScript III Reverse Transcriptase (ThermoFisher Scientific, Monza, Italy). Human fibroblast cDNAs from Hunter syndrome patients or healthy controls, were obtained from the Biobank at G. Gaslini Institute (Genova). For the RT-qPCRs, the quantitative expression for each marker was determined in patients RNA sample by comparing it to that of pooled fibroblasts RNAs from 10 healthy subjects.

The cDNAs were subsequently subjected to SYBR Green-based real-time PCR using a RotorGene 3000 (Corbett, Concorde, NSW). Primers are listed in Table 2.

RT-qPCR data were analyzed using a manually set threshold and the baseline was set automatically to obtain the threshold cycle (Ct) value for each target. As endogenous housekeeping control genes for normalization, GAPDH for zebrafish and human samples and B2M for mouse samples have been used. Relative gene expression among samples was determined using the comparative Ct method (2–ΔΔCt). Results are expressed as the mean ± SD relative expression. All statistical analysis were perfomed using GraphPad Prism 5.0 software.

Western blot

All procedures were performed as described previously (27). For mouse and fish bone samples, lysis in Tissue Extraction Reagent (ThermoFisher Scientific, Monza, Italy) was carried out for 2 days in the presence of protease inhibitor (ThermoFisher Scientific, Monza, Italy) and phosphatase Inhibitor Cocktails 2 and 3 (Sigma-Aldrich, Milan, Italy), The lysates were centrifuged at 13000*g* for 30 min at 4°C. The supernatant was collected and protein concentration was determined by the Bradford method. Extracted proteins were supplemented with 4× sample buffer, heated at 70°C for 10 min and run onto precast SDS-PAGE (ThermoFisher Scientific, Monza, Italy). Proteins were transferred on Immobilon-P membranes (Merk Millipore, Italy) in 25 mM Tris, 192 mM glycine, 20% methanol (v/v), 0.1% SDS. Membranes were incubated overnight with primary antibodies against the following proteins: Gli1 (#2534; Cell signaling Biotechnology, Danvers, USA), β-actin (SC59459; Santa Cruz Biotechnology, Dallas, USA), bglap (SC30045; Santa Cruz Biotechnology, Dallas, USA), col10a1 (SC323750; Santa Cruz Biotechnology, Dallas, USA), pea3 (ab189826 Abcam, Cambridge, UK), GAPDH (ab 9485, Abcam. Cambridge, UK). All antibodies were used at 1: 1000 dilution. HRP Chemiluminescence signals were detected by Kodak Image Station 4000MMpro (Eastman Kodak, New Haven, CT) and analyzed with the Kodak Image software.

Generation of stable Ids$^{-/-}$ mutant fish

The CRISPR/Cas9 technique, following a previously described protocol was used (41). The PCS2-cas9 and pT7cas9sgRNA2 plasmids were purchased from Addgene (Cambridge, MA, USA). A target sequence in the first and second exon of the *ids* was chosen using CHOPCHOP software (https://chopchop.rc.fas.harvard.edu/).The sequence was: GTTAGGAAAGACACTCTACT AGG. To create a double-stranded oligo to be cloned in the gRNA plasmid, two single-stranded oligos have been produced according to previous published guidelines (41). The sequences of the two oligos are: 5′-TAGGTAGGAAAGACACTCTACT-3′ and 5′-ATCCTTTCTGTGAGATGACAAA-3′. Cas9 mRNA and the gRNA have been transcribed and co-injected in one cell-stage embryos, with concentrations of 30 ng/μl for gRNA and 100 ng/μl for Cas9, respectively.

Whole-mount Alcian blue Alizarin red staining

Mice at postnatal stages (P7 and P14) were sacrificed by and skin and organs removed. Fixation was carried out in 95% ethanol for 5 days. Samples were washed with water and stained with 1% Alcian blue at pH 1.0 for 3 days. Mice samples were re-fixed with 95% ethanol overnight and put in 1% KOH solution for 5 days. After several washes with water, a solution of Alizarin red 1% pH 4.2 was added for 5 days. Samples were washed with 1% KOH and stored in glycerol. For zebrafish samples, fish larvae were fixed 1 h at room temperature in 4% buffered paraformaldehyde, washed in 50% ethanol and dehydrated overnight in 95% ethanol. Staining was carried out in Alizarin solution (0.25%, w/v, in 2% KOH) for 3 h and larvae were then briefly cleared in 2% KOH (w/v) and stored in KOH/glycerol (20: 80). For mouse specimens, mice were sacrificed and skin and organs were removed. Fixation was carried out in 95% ethanol for 5 days. Samples were washed with water and stained with 1% Alcian blue at pH 1.0 for 3 days. Mice samples were re-fixed with 95% ethanol overnight and put in 1% KOH solution for 5 days. After several washes with water, a solution of Alizarin red 1% pH 4.2 was added for 5 days. Samples were washed with 1% KOH and stored in glycerol.

Paraffin embedding and sectioning

Mouse samples were fixed in 4% PFA in PBS, washed in PBS and dehydrated in ethanol solutions of increasing concentrations. Before dehydration, mice bones were decalcified using a solution of 10% EDTA in PBS and samples were dehydrated in xylene. All solutions were removed and paraffin embedding was carried out. Sectioning was performed using a microtome and tissue sections were collected on SuperfrostPlus slides.

Alcian blue-nuclear fast red staining

Tissue sections were deparaffinized with xylene and rehydrated with ethanol solutions of decreasing concentration. After several washes with distilled water, a 0.1 M citric acid solution was added to the samples for 3 min. Sections were stained with 1% pH 1.0 Alcian blue for 20 min. After several washes with distilled water, a nuclear-fast-red solution was added to the samples for 10 min. Sections were washed and dehydrated with ethanol solutions of increasing concentration and mounted for histological analysis.

Table 2. List of primers and their relative targets used for the RT-qPCR analysis

	Primer	RefSeq
Zebrafish gene		
d2GFP For	TAAACGGCCACAAGTTCAGC	–
d2GFP Rev	AAGTCGTGCTGCTTCATGTG	–
pea3(etv4) For	CGATGAGCAGTTTGTTCCTG	NM_131425
pea3(etv4) Rev	CTTGTGGCTGCAGGACTG	NM_131425
erk1(mapk3) For	TGACCCTGAACATGACCACA	NM_201507
erk1(mapk3) Rev	GGTCCAGATAGTGCTTCCCA	NM_201507
erm1(etv5b) For	TGTTCCAGATTTCCAGTCGG	NM_001309209
erm1(etv5b) Rev	AGTCTCTGCTCTTGTCCACA	NM_001309209
col2a1 For	AAGGGTGAGGCAGGTTCTAAC	NM_131292
col2a1 Rev	GCAGACCATCATTACCACGG	NM_131292
col10a1a For	CCGCAGTACCAGCCTTACTC	NM_001083827
col10a1a Rev	TTTCCAGGTGCTGAATACCC	NM_001083827
bglap For	TGAAGAGCCTGACAGTCCTG	NM_001083857
bglap Rev	GTTCCAGCCCTCTTCTGTCT	NM_001083857
osx(sp7) For	AATCAGCTCGTGGTTCTGGA	NM_212863
osx(sp7) Rev	GCTTTCAGATGCGAGGCTTT	NM_212863
gapdh For	GTGCAGGAGGCATTGCTTACA	NM_001115114
gapdh Rev	GTGGAGTCTACTGGTGTCTTC	NM_001115114
Mouse gene		
Col2a1 For	AAGGGTCACAGAGGTTACCC	NM_031163
Col2a1 Rev	GTCCTCTCTCACCAGGCAG	NM_031163
Bglap For	GAGGGCAATAAGGTAGTGAACAGA	NM_007541
Bglap Rev	AAGCCATACTGGTTTGATAGCTCG	NM_007541
Col10a1 For	ATGCTGAACGGTACCAAACG	NM_009925
Col10a1 Rev	GGAATGCCTTGTTCTCCTCT	NM_009925
Il1b For	ACCTGTGTCTTTCCCGTGGAC	NM_008361.4
Il1b Rev	GGGAACGTCACACACCAGCA	NM_008361.4
Tnfa For	AGCCCACGTCGTAGCAAACC	NM_013693.3
Tnfa Rev	CATCGGCTGGCACCACTAGT	NM_013693.3
Pea3(Etv4) For	CCTTCTGCAGCAAATCTCCC	NM_001316365
Pea3Etv4 Rev	CTGCTCATCACTGTCCGGTA	NM_001316365
Erk1(Mapk3) For	TACGGCATGGTCAGCTCAG	NM_011952
Erk1(Mapk3) Rev	AGGATGTCTCGGATGCCTATAA	NM_011952
Dusp6 For	ATGCGGGCGAGTTCAAATAC	NM_026268
Dusp6 Rev	CAAGCAATGCACCAGGACAC	NM_026268
B2m For	CGGCCTGTATGCTATCCAGA	NM_009735
B2m Rev	ATTTCAATGTGAGGCGGGTG	NM_009735
Human gene		
DUSP6 For	CGTTCTACCTGGAAGGTGGC	NM_001946
DUSP6 Rev	CCGAGGAAGAGTCAGAGCTG	NM_001946
ERK1(MAPK3) For	CAACCACATTCTGGGCATCC	NM_002746
ERK1(MAPK3) Rev	CTTGGTCTTGGAGGGCAGAG	NM_002746
PEA3(ETV4) For	CTACACCTTCAGCAGCAAATCG	NM_001079675
PEA3(ETV4) Rev	TCACTGTCTGGTACCTGAGCTTC	NM_001079675
GAPDH For	CGAGCCACATCGCTCAGAC	NM_002046
GAPDH Rev	ACAATATCCACTTTACCAGAGTTA AAAGC	NM_002046

Immunohistochemistry

Immunohystochemistry analysis was carried out on paraffin-embedded sections. Sections were deparaffinized with xylene and progressively rehydrated with ethanol solutions in phosphate-buffered saline (PBS). Antigen retrieval was achieved with 1 mM pH 6.0 sodium citrate using a steam chamber. The primary antibody (PEA3, GeneTex, Irvine, CA, USA, 1: 100 dilution) (COL2A1, Santa Cruz Biotechnology, Dallas, TX, USA, 1: 100 dilution) was incubated overnight at 4°C, while the secondary antibody (goat anti rabbit-alkaline phosphatase, Sigma, 1: 200) was incubated 1 h at room temperature and NBT-BCIP staining (ThermoFisher Scientific, Monza, Italy) was performed according to manufacturer's instructions.

Microscopy and image analysis

Transgenic fluorescent zebrafish were analyzed using a Leica M165FC microscope (Leica, Milan, Italy). All images were acquired with a Nikon DS-F12 digital camera. Confocal zebrafish images were acquired with a Nikon C2 H600L confocal microscope (Nikon, Florence, Italy), while stained slides from mouse sample were acquired with Leica DMR compound/Normarski microscope (Leica, Milan, Italy). For all images the same exposure parameters were chosen and analyzed using ImageJ program or Imaris software. Statistical analyses were carried out with Prism software (GraphPad).

MicroCT

Each control ($n = 4$) and $ids^{ia200/ia200}$ ($n = 4$) fish was placed in a cylindrical polyethylene container (i.e. diameter of 1.1 cm) with saline solution to avoid dehydration and was analyzed by an ex vivo high-resolution Micro-CT 1172 (Skyscan, Aartselaar, Belgium). The following MicroCT parameters were applied: 59 kV of voltage, 167 μA of current, 1 mm aluminum filter to reduce beam-hardening artifacts, 17 μm of isotropic voxel size and 1280 × 1024 pixel of field of view. All samples underwent a 180° rotation, with a 0.7 rotation step and a frame averaging of 2. Each scan required about 4 h. The acquired raw data were reconstructed with the N-Recon Software (Skyscan, Aartselaar, Belgium). The bitmap images obtained after the reconstruction were then converted in Dicom files (Dicom Converter, Skyscan, Aartselaar, Belgium). Three-dimensional (3D) and MPRs were performed by CTVox (Skyscan, Aartselaar, Belgium) and Horos (Open Source Software, https://www.horosproject.org), respectively.

Supplementary Material

Supplementary Material is available at *HMG* online.

Acknowledgements

We thank Dr Martina Milanetto and Dr Luigi Pivotti for the care of fish husbandry and M.Tsang (University of Pittsburgh, PA, USA) for providing the *Tg(Dusp6: d2EGFP)*^{pt6} line.

Conflict of Interest statement: None declared.

Funding

This work has been partly financially supported by the Italian Ministry of Health (Ricerca Finalizzata GR-2008-1139743) and BIRD 2017 (University of Padova) to E.M and by unrestricted grants from "Cinque per mille e Ricerca Corrente", "Ministero della Salute" to SL and MF. Patient samples were obtained from the "Cell Line and DNA Biobank from patients affected by Genetic Diseases" (Istituto Giannina Gaslini), member of Telethon Network of Genetic Biobanks (project no. GTB12001).

References

1. Settembre, C., Fraldi, A., Medina, D.L. and Ballabio, A. (2013) Signals from the lysosome: a control centre for cellular clearance and energy metabolism. *Nat. Rev. Mol. Cell Biol.*, **14**, 283–296.
2. Ballabio, A. and Gieselmann, V. (2009) Lysosomal disorders: from storage to cellular damage. *Biochim. Biophys. Acta*, **1793**, 684–696.
3. Heppner, J.M., Zaucke, F. and Clarke, L.A. (2015) Extracellular matrix disruption is an early event in the pathogenesis of skeletal disease in mucopolysaccharidosis I. *Mol. Genet. Metab.*, **114**, 146–155.
4. Wraith, J.E., Scarpa, M., Beck, M., Bodamer, O.A., De Meirleir, L., Guffon, N., Meldgaard Lund, A., Malm, G., Van der Ploeg, A.T. and Zeman, J. (2008) Mucopolysaccharidosis type II (Hunter syndrome): a clinical review and recommendations for treatment in the era of enzyme replacement therapy. *Eur. J. Pediatr.*, **167**, 267–277.
5. Martin, R., Beck, M., Eng, C., Giugliani, R., Harmatz, P., Munoz, V. and Muenzer, J. (2008) Recognition and diagnosis of mucopolysaccharidosis II (Hunter syndrome). *Pediatrics*, **121**, e377–e386.
6. Moro, E., Tomanin, R., Friso, A., Modena, N., Tiso, N., Scarpa, M. and Argenton, F. (2010) A novel functional role of iduronate-2-sulfatase in zebrafish early development. *Matrix Biol.*, **29**, 43–50.
7. Lu, P., Takai, K., Weaver, V.M. and Werb, Z. (2011) Extracellular matrix degradation and remodeling in development and disease. *Cold Spring Harb. Perspect. Biol.*, **3**, a005058.
8. Clarke, L.A. (2011) Pathogenesis of skeletal and connective tissue involvement in the mucopolysaccharidoses: glycosaminoglycan storage is merely the instigator. *Rheumatology (Oxford)*, **50**, v13–v18.
9. Simonaro, C.M., D'Angelo, M., Haskins, M.E. and Schuchman, E.H. (2005) Joint and bone disease in mucopolysaccharidoses VI and VII: identification of new therapeutic targets and biomarkers using animal models. *Pediatr. Res.*, **57**, 701–707.
10. Peck, S.H., Casal, M.L., Malhotra, N.R., Ficicioglu, C. and Smith, L.J. (2016) Pathogenesis and treatment of spine disease in the mucopolysaccharidoses. *Mol. Genet. Metab.*, **118**, 232–243.
11. Kingma, S.D.K., Wagemans, T., IJlst, L., Bronckers, A.L.J.J., van Kuppevelt, T.H., Everts, V., Wijburg, F.A. and van Vlies, N. (2016) Altered interaction and distribution of glycosaminoglycans and growth factors in mucopolysaccharidosis type I bone disease. *Bone*, **88**, 92–100.
12. Ornitz, D.M. and Marie, P.J. (2002) FGF signaling pathways in endochondral and intramembranous bone development and human genetic disease. *Genes Dev.*, **16**, 1446–1465.
13. Cinque, L., Forrester, A., Bartolomeo, R., Svelto, M., Venditti, R., Montefusco, S., Polishchuk, E., Nusco, E., Rossi, A., Medina, D.L. *et al.* (2015) FGF signalling regulates bone growth through autophagy. *Nature*, **528**, 272–275.
14. Teven, C.M., Farina, E.M., Rivas, J. and Reid, R.R. (2014) Fibroblast growth factor (FGF) signaling in development and skeletal diseases. *Genes Dis.*, **1**, 199–213.
15. Raman, R., Venkataraman, G., Ernst, S., Sasisekharan, V. and Sasisekharan, R. (2003) Structural specificity of heparin binding in the fibroblast growth factor family of proteins. *Proc. Natl. Acad. Sci. U.S.A.*, **100**, 2357–2362.
16. Spoorendonk, K.M., Peterson-Maduro, J., Renn, J., Trowe, T., Kranenbarg, S., Winkler, C. and Schulte-Merker, S. (2008) Retinoic acid and Cyp26b1 are critical regulators of osteogenesis in the axial skeleton. *Development*, **135**, 3765–3774.
17. Moro, E., Vettori, A., Porazzi, P., Schiavone, M., Rampazzo, E., Casari, A., Ek, O., Facchinello, N., Astone, M. and Zancan, I. (2013) Generation and application of signaling pathway reporter lines in zebrafish. *Mol. Genet. Genomics*, **288**, 231–242.
18. Molina, G.A., Watkins, S.C. and Tsang, M. (2007) Generation of FGF reporter transgenic zebrafish and their utility in chemical screens. *BMC Dev. Biol.*, **7**, 62.
19. Hammond, C.L. and Moro, E. (2012) Using transgenic reporters to visualize bone and cartilage signaling during development in vivo. *Front. Endocrinol.*, **3**, 91.
20. Garcia, A.R., Pan, J., Lamsa, J.C. and Muenzer, J. (2007) The characterization of a murine model of mucopolysaccharidosis II (Hunter syndrome). *J. Inherit. Metab. Dis.*, **30**, 924–934.
21. Opoka-Winiarska, V., Jurecka, A., Emeryk, A. and Tylki-Szymańska, A. (2013) Osteoimmunology in mucopolysaccharidoses type I, II, VI and VII. (2013) Immunological regulation of the osteoarticular system in the course of metabolic inflammation. *Osteoarthritis Cartilage*, **21**, 1813–1823.
22. Kim, S.H., Turnbull, J. and Guimond, S. (2011) Extracellular matrix and cell signalling: the dynamic cooperation of integrin, proteoglycan and growth factor receptor. *J. Endocrinol.*, **209**, 139–151.
23. Batzios, S.P., Zafeiriou, D.I. and Papakonstantinou, E. (2013) Extracellular matrix components: an intricate network of possible biomarkers for lysosomal storage disorders? *FEBS Lett.*, **587**, 1258–1267.
24. Rozario, T. and DeSimone, D.W. (2010) The extracellular matrix in development and morphogenesis: a dynamic view. *Dev. Biol.*, **341**, 126–140.
25. Platt, F.M., Boland, B. and van der Spoel, A.C. (2012) The cell biology of disease: lysosomal storage disorders: the cellular impact of lysosomal dysfunction. *J. Cell Biol.*, **199**, 723–734.
26. Su, N., Jin, M. and Chen, L. (2014) Role of FGF/FGFR signaling in skeletal development and homeostasis: learning from mouse models. *Bone Res.*, **2**, 14003.
27. Costa, R., Urbani, A., Salvalaio, M., Bellesso, S., Cieri, D., Zancan, I., Filocamo, M., Bonaldo, P., Szabò, I., Tomanin, R. and Moro, E. (2017) Perturbations in cell signaling elicit early cardiac defects in mucopolysaccharidosis type II. *Hum. Mol. Genet.*, **26**, 1643–1655.
28. Scarpa, M., Almássy, Z., Beck, M., Bodamer, O., Bruce, I.A., De Meirleir, L., Guffon, N., Guillén-Navarro, E., Hensman, P., Jones, S. *et al.* (2011) Mucopolysaccharidosis type II: European recommendations for the diagnosis and multidisciplinary management of a rare disease. *Orphanet. J. Rare Dis.*, **6**, 72.
29. Parini, R., Rigoldi, M., Tedesco, L., Boffi, L., Brambilla, A., Bertoletti, S., Boncimino, A., Del Longo, A., De Lorenzo, P., Gaini, R. *et al.* (2015) Enzymatic replacement therapy for

Hunter disease: up to 9 years' experience with 17 patients. *Mol. Genet. Metab. Rep.*, **3**, 65–74.
30. Howe, L.R., Crawford, H.C., Subbaramaiah, K., Hassell, J.A., Dannenberg, A.J. and Brown, A.M. (2001) PEA3 is up-regulated in response to Wnt1 and activates the expression of cyclooxygenase-2. *J. Biol. Chem.*, **276**, 20108–20115.
31. Tumova, S., Woods, A. and Couchman, J.R. (2000) Heparan sulfate proteoglycans on the cell surface: versatile coordinators of cellular functions. *Int. J. Biochem. Cell Biol.*, **32**, 269–288.
32. Haugsten, E.M., Sorensen, V., Brech, A., Olsnes, S. and Wesche, J. (2005) Different intracellular trafficking of FGF1 endocytosed by the four homologous FGF receptors. *J. Cell Sci.*, **118**, 3869–3881.
33. Inoue, D. and Wittbrodt, J. (2011) One for all–a highly efficient and versatile method for fluorescent immunostaining in fish embryos. *PLoS One*, **6**, e19713.
34. Hammond, C.L. and Schulte-Merker, S. (2014) Two populations of endochondral osteoblasts with differential sensitivity to Hedgehog signals. *Development*, **120**, 1643–1655.
35. Thisse, C., Thisse, B., Schilling, T.F. and Postlethwait, J.H. (1993) Structure of the zebrafish snail1 gene and its expression in wild-type, spadetail and no tail mutant embryos. *Development*, **119**, 1203–1215.
36. Kiefer, P., Mathieu, M., Mason, I. and Dickson, C. (1996) Secretion and mitogenic activity of zebrafish FGF3 reveal intermediate properties relative to mouse and Xenopus homologues. *Oncogene*, **12**, 1503–1511.
37. Schulte-Merker, S., van Eeden, F.J., Halpern, M.E., Kimmel, C.B. and Nusslein-Volhard, C. (1994) No tail (ntl) is the zebrafish homologue of the mouse T (Brachyury) gene. *Development*, **120**, 1009–1015.
38. Znosko, W.A., Yu, S., Thomas, K., Molina, G.A., Li, C., Tsang, W., Dawid, I.B., Moon, A.M. and Tsang, M. (2010) Overlapping functions of Pea3 ETS transcription factors in FGF signaling during zebrafish development. *Dev. Biol.*, **342**, 11–25.
39. Reifers, F., Bohli, H., Walsh, E.C., Crossley, P.H., Stainier, D.Y. and Brand, M. (1998) Fgf8 is mutated in zebrafish acerebellar (ace) mutants and is required for maintenance of midbrain-hindbrain boundary development and somitogenesis. *Development*, **125**, 2381–2395.
40. Furthauer, M., Reifers, F., Brand, M., Thisse, B. and Thisse, C. (2001) sprouty4 acts in vivo as a feedback-induced antagonist of FGF signaling in zebrafish. *Development*, **128**, 2175–2186.
41. Jao, L.E., Wente, S.R. and Chen, W. (2013) Efficient multiplex biallelic zebrafish genome editing using a CRISPR nuclease system. *Proc. Natl. Acad. Sci. U.S.A.*, **110**, 13904–13909.